Effect of Silicone Patch Containing Metal-organic Framework on Hypertrophic Scar Suppression

XIN RUI ZHANG[1†], UNJIN RYU[2†], BAKHTIYOR NAJMIDDINOV[1], THUY-TIEN THI TRINH[3],
KYUNG MIN CHOI[2,4†], SUN-YOUNG NAM[1†] and CHAN YEONG HEO[1,3,5†]

[1]*Department of Plastic and Reconstructive Surgery, Seoul National University Hospital,*
Seoul National University College of Medicine, Seoul, Republic of Korea;
[2]*Department of Chemical and Biological Engineering, Sookmyung Women's University, Seoul, Republic of Korea;*
[3]*Korean Institute of Nonclinical Study, H&Bio. Co. Ltd., Seongnam, Republic of Korea;*
[4]*R&D Center, LabInCube Co. Ltd., Cheongju, Republic of Korea;*
[5]*Department of Medical Device Development, College of Medicine,*
Seoul National University, Seoul, Republic of Korea

Abstract. *Background/Aim: Hypertrophic scars (HS) are an abnormal cutaneous condition of wound healing characterized by excessive fibrosis and disrupted collagen deposition. This study assessed the potential of a silicone patch embedded with chemically stable zirconium-based metal-organic frameworks (MOF)-808 structures to mitigate HS formation using a rabbit ear model. Materials and Methods: A silicone patch was strategically engineered by incorporating Zr-MOF-808, a composite structure comprising metal ions and organic ligands. Structural integrity of the Zr-MOF-808 silicone patch was validated using scanning electron microscopy and X-ray diffraction analysis. The animals were divided into three groups: a control, no treatment group (Group 1), a silicone patch treatment group (Group 2), and a group treated with a 0.2% loaded Zr-MOF-808 silicone patch (Group 3). HS suppression effects were quantified using scar elevation index (SEI), dorsal skin thickness measurements, and myofibroblast protein expression. Results: Histopathological examination of post-treatment HS samples revealed substantial reductions in SEI (34.6%) and epidermal thickness (49.5%) in Group 3. Scar hyperplasia was significantly diminished by 53.5% (p<0.05), while collagen density declined by 15.7% in Group 3 compared to Group 1. Western blot analysis of protein markers, including TGF-β1, collagen-1, and α-SMA, exhibited diminished levels by 8.8%, 12%, and 21.3%, respectively, in Group 3, and substantially higher levels by 21.9%, 27%, and 39.9%, respectively, in Group 2. On the 35th day post-wound generation, Zr-MOF-808-treated models exhibited smoother, less conspicuous, and flatter scars. Conclusion: Zr-MOF-808-loaded silicone patch reduced HS formation in rabbit ear models by inducing the proliferation and remodeling of the wound healing process.*

[†]These Authors contributed equally to this study.

Correspondence to: Kyung Min Choi, Department of Chemical and Biological Engineering, Sookmyung Women's University, 100 Cheongpa-ro 47-gil, Yongsan-gu, Seoul 04310, Republic of Korea; Sun-Young Nam, Department of Plastic & Reconstructive Surgery, Seoul National University Bundang Hospital, Seongnam, 13620, Republic of Korea; Chan Yeong Heo, Department of Plastic and Reconstructive Surgery, College of Medicine, Seoul National University, Seoul 03080, Republic of Korea. E-mail: kmchoi@sookmyung.ac.kr (K.M. Choi), 99261@snubh.org (S.Y. Nam), lionheo@snu.ac.kr (C.Y. Heo)

The skin is a complex, multi-layered organ within the integumentary system, which functions as a resilient outer barrier safeguarding the underlying musculature, skeletal structures, neural networks, and internal organs. It constitutes the foremost line of defense against a myriad of external adversities. Various injurious factors, such as trauma, thermal burns, and surgical procedures, can precipitate the formation of cutaneous skin wounds. The emergence of hypertrophic scars (HS) may subsequently interfere with normal skin functionality, potentially causing anxiety and various associated psychological disorders (1, 2). The cause of HS has been reported to be a consequence of several previously reported incidences. These incidence rates range from 40% to 94% after surgical operations and from 30% to 91% after

burn injuries (3). HS is an anomalous cutaneous condition in response to wound healing that is extremely thickened and has abnormal collagen build-up and is distinguished by thickened, elevated, and itchy rigid painful scars, which significantly impact the quality of life (4, 5). HS are also known to induce functional sequelae, accompanied by a decrease in cosmetic appearance, diminished skin elasticity, and restricted mobility of adjacent joints, thereby significantly affecting patients afflicted with hypertrophic scarring (6, 7). The skin is the main human-environment interface and is therefore more likely to be harmed. Scar formation is a natural, complex, and tightly-regulated process involving cell migration, inflammation, innervation, and angiogenesis (8). However, a pathological healing phase, which is marked by excessive fibrosis, can lead to a disorganized formation. The presence of real wounds results in pathological fibrosis as long as the tissue has an inflammatory response. This inflammatory response can help proliferative conditions in fibroblasts that can be triggered by continued extracellular matrix deposition created by fibroblasts and myofibroblasts for long periods, and can therefore be sustained (9).

Dysregulation of TGF-β/Smad signaling is a major factor in scarring and fibrosis, leading to aberrant synthesis and deposition of collagen (10-12). The myofibroblast phenotype (especially TGF-β) is responsible for major collagen deposition and wound contraction (13). Although treatment techniques of scars are not well known, in the last decade, drug therapy and silicone gel sheets have become the most popular recovery therapies for HS (14). Although various treatment options (such as corticosteroid injections, surgical excision, laser/drug/radiation/compression/gene therapy, silicone gel membrane, and interferon injection) are available, it is very difficult to prevent HS tissue formation and maintain safe tissue regeneration (15, 16). Silicone gel sheeting is the most common first-line therapy that can improve stratum corneum hydration, thereby helping to regulate the production of fibroblasts and to reduce collagens (17, 18). The silicone gel sheet treatment is expected to commence approximately 2 weeks after complete healing. The duration of the application of silicone gel sheets usually varies from 12 to 24 h per day, after which they are washed and reapplied (19).

The porous sub-types of polymers are considered as metal-organic frameworks (MOFs), which consist of inorganic metal ions or clusters linked by polydentate organic ligands, forming one, two, or three-dimensional structures (20, 21). Since Hoskins and Robson discovered MOFs in 1989, they have been used for gas adsorption and separation, catalysis, luminescence, sensing, and proton conductivity (22-27). Because of their versatile structure and composition, various functions, strong biocompatibility, high drug loads, and inherent biodegradability, such biomaterials

gained interest in the therapeutic field (28-32). Based on this wide range of MOFs' biological benefits and functions, in the current study, we investigated the effectiveness of zr-MOF-808 in HS treatment. The present study aimed to assess the use of a silicone patch containing Zr-MOF-808 to diminish HS after post-operative procedures in a rabbit model, which can produce lesions similar to human HS.

Materials and Methods

Materials. Zirconium (IV) chloride oxide octahydrate ($ZrOCl_2 \cdot 8H_2O$, 99%) was purchased from Junsei Chemical Co., Ltd. (Tokyo, Japan). Trimesic acid (95%), N, N-dimethylformamide (DMF, 99.8%), and formic acid (96%) were purchased from Sigma-Aldrich (St. Louis, MO, USA).

MOF-808 ($Zr_6O_4(OH)_4(BTC)_2(HCOO)_6$) preparation. The modified synthetic MOF-808 was synthesized as described previously by Jiang *et al*. (33), with the solution for ligand and metal prepared separately. For the metal solution, N, N-dimethylformamide (DMF, 112.5 ml), formic acid (225 ml), and $ZrOCl_2 \cdot 8H_2O$ (4.8 g, 15 mmol) were mixed in a 500 ml glass jar. For the preparation of the ligand, only trimesic acid was dissolved in DMF solution (112.5 ml). Each solution was well dissolved by sonication and the ligand solution was blended with a metal solution after checking its consistency. The mixture was incubated at 130˚C for 48 h, cooled to room temperature, and centrifuged at 5,200 × *g* for 10 min. The white solid pellet was collected and washed thrice with DMF. The obtained product was dissolved in DMF for three days and subsequently soaked in a mixture of water and acetone for another three days. The fresh solvent was replaced three times per day. The final product was dried, washed, and placed in a desiccator.

Silicone patch preparation using MOF-808. The MOF-808 tackiness silicone patch preparation is subdivided into two parts: silicone adhesive surface preparation and protective film preparation. To prepare the silicone adhesive surface, the mixture of polysiloxane with a vinyl group (10-100 wt.%), dimethyl silicone oil (5-40 wt.%), polysiloxane with Si-H bond (1-50 wt.%), silicone resin (0.5-20 wt.%), platinum (Pt) catalyst (0.1-5 wt.%), and MOF-808 (0.2 wt.%) was blended by a mechanical stirrer at 1,000 to 3,000 rpm. The MOF particles were spread under a decreased pressure (<0.1 MPa) for 1-2 h. The same method was applied in the preparation of the control sample with the absence of MOF-808.

The protective film was prepared on the silicone adhesive side using a polyurethane solution consisting of moisture-permeable waterproof material and a solvent, which was formed on a release paper. The silicone film was made with silicone resin and a solvent on the release paper. Finally, the silicone patch containing MOF-808 was prepared by uniformly adding a silicone formula to the protective film.

Characterization of MOF-808 loaded silicone patch. The characteristics of the MOF-808 contained silicone patch were investigated using scanning electron microscopy (SEM) (JSM-7600F, JEOL, Tokyo, Japan). In GB LOW mode, SEM imaging was performed with a WD of 8.0 mm and scanned at 3 kV to observe the surface morphologies of MOF-808 and the silicone sheet. Cross-section SEM images were analyzed using focused ion beam/SEM
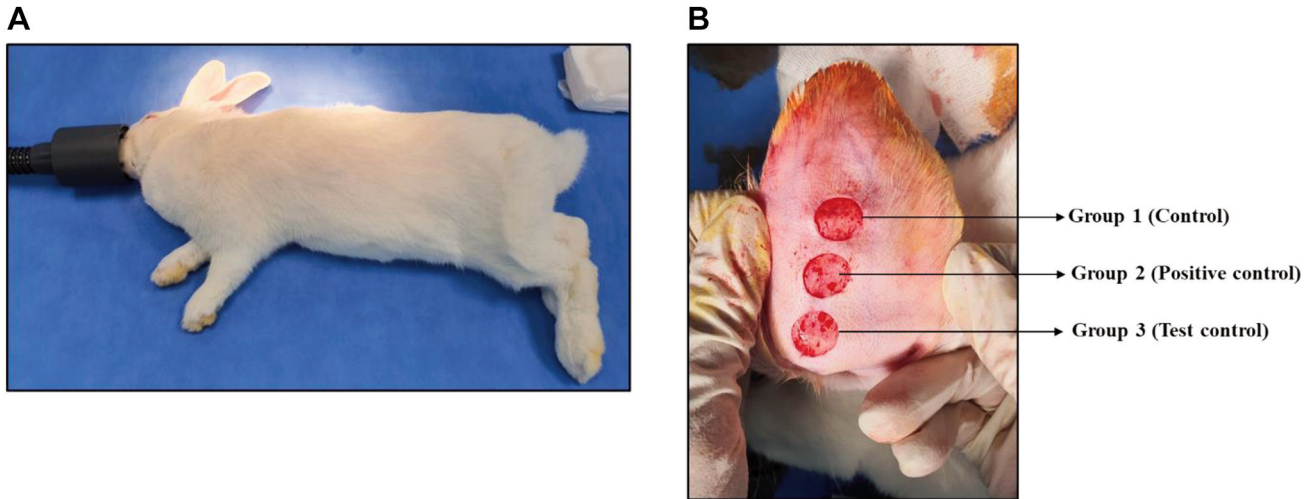
A

B

Figure 1. *Establishment of hypertrophic scar model. (A) The wound establishment surgery was performed under general anesthesia of the rabbits. (B) Three circular (1.2 cm in diameter) lesions were made while the ear cartilage was preserved on the ventral surface of the left ear of each rabbit. Group 1 is the control group, receiving no therapy; Group 2 is the positive control group, receiving a silicone patch treatment without MOF-808; and Group 3 is the experimental group, receiving a silicone patch treatment with 0.2% MOF-808.*

(FIB/SEM, Quanta™ 3D FEG, FEI). A Bruker advanced diffractometer D8 (Cu Kα Radiation α=1.54056 Å) was used to track powder X-ray diffraction patterns (PXRD). The samples were kept in a silicone holder and continuously scanned at a speed of 5°/min (40 KV, 40 mA).

In vivo hypertrophic scar model. A hypertrophic scar model was developed using five young adult New Zealand White female rabbits weighing approximately 3 to 4 kg. All experiments were performed in accordance with the approved procedures from the Bundang Hospital Animal Experimental Center Animal Care and Use Committee of the Seoul National University under the approval number BA-1911-284-086-01. All the methodological procedures were performed in accordance with the National Institutes of Health (NIH) Animal Care and Use Guide. General anesthesia was administered to the rabbit models before wound establishment surgery (Figure 1A). Three circular full-thickness wounds of approximately 12 mm in diameter were created on the bare cartilage on the ventral surface of the left ear of each rabbit (Figure 1B). Ketamine and xylazine chemicals were used to anesthetize the rabbits. For each wound, a dissecting microscope was used to remove the epidermis, dermis, and perichondrium with intact ear cartilage, using a dermal punch, surgical blade, and scissors. Group 1 was the control group, where no treatment was provided, group 2 was the positive control group that was treated with a silicone patch (Wonbiogene Co. Ltd., Gumi, Republic of Korea), and group 3 was the test group, which was treated with 0.2% Zr-MOF-808 loaded silicone patch. After two weeks of self-healing, the developed HS of each testing group was treated with the indicated treatment, the silicone patches were applied every day for three weeks continuously.

At day 35th post-wound generation, the photographs of the HS regions were obtained, and animals were anesthetized and sacrificed for collection of the scar samples. All specimens were fixed and preserved in 10% formalin immediately after collection for subsequent analysis.
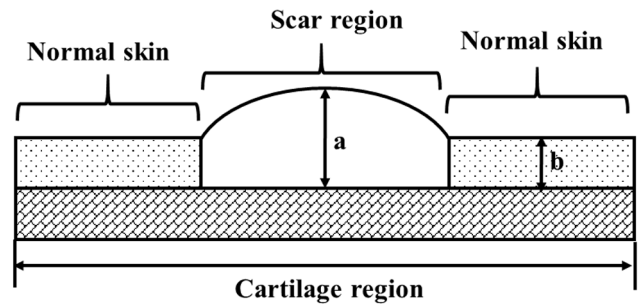

Figure 2. *An illustration of the scar elevation index (SEI) measurement. (A) is the height from the peak of HS to the cartilage and (B) is the distance from the surface of normal skin to the cartilage.*

Quantification of HS by scar elevated index (SEI). The paraffin-embedded samples (5 μm thickness) were stained with hematoxylin and eosin (H&E) to assess the SEI and epidermal thickness. Following the previously described procedure, the images were photographed at 10× magnification to assess the SEI under a light microscope (Carl Zeiss, Baden-Württemberg, Germany) for further analysis of the scar elevation (34). The hypertrophy degree in each scar was indicated as the SEI value calculated as the ratio between the height of the tissue in the overall area of injury and the height of the tissue text to the scar (35). A diagrammatic representation of the SEI is shown in Figure 2. The epidermal thickness was analyzed under 40× magnification. The scar hyperplasia rate was estimated using ImageJ software (National Institutes of Health, Bethesda, MA, USA). The experiment was performed in triplicate, and the results are presented as the average mean value and standard deviation.

Quantification of collagen fibers. Tissue sections were stained with Masson's Trichrome to evaluate the arrangement of collagen fibers.
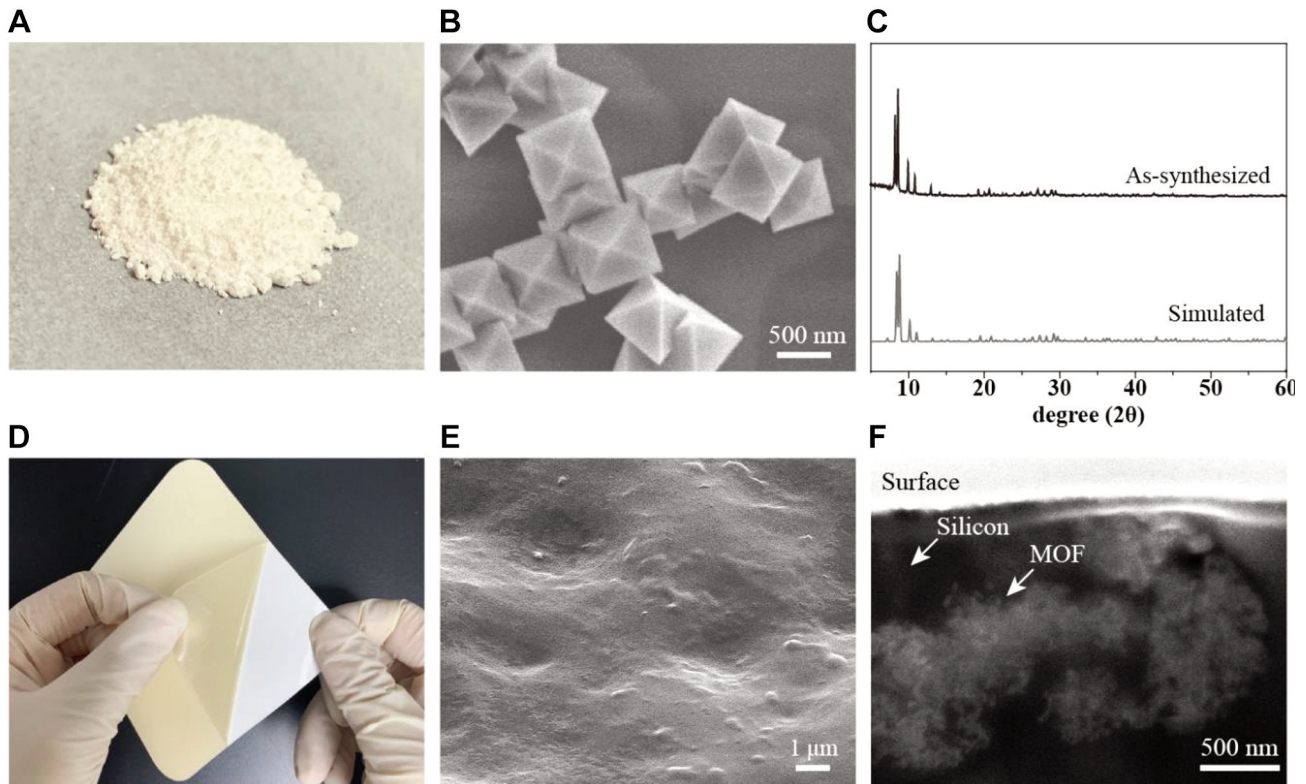
Figure 3. *Characterization of MOF-808 particles and MOF-808 loaded silicone patch. (A) A digital image of the powdered MOF-808. (B) MOF-808 particles are observed in a SEM image (scale bar: 1 μm). (C) Comparison of X-ray diffraction patterns of as-synthesized MOF-808 (The upper black line) and simulated MOF-808 (The bottom gray line) (56). (D) Digital image of 0.2% MOF-loaded silicone patch. (E - F) top (E) and the cross-section view (F) SEM images of 0.2% MOF loaded silicone patch.*

Briefly, the slides were dehydrated twice in 100% ethanol for 3 min, and then in 95% ethanol for 3 min. The sections were fixed overnight in Bouin's fixative solution at room temperature, rinsed with tap water, and stained with Weigert's iron hematoxylin working solution for 10 min. After washing with water for 10 min, all the slides were incubated in Biebrich scarlet-acid fuschin solution for 5 min followed by 10 min inoculation with the phosphomolybdic-phosphotungstic acid solution. After inoculation, the samples were stained with an aniline blue solution for 5 min and rinsed in 1% acetic acid for 1 min. Finally, the sections were mounted using a mounting solution. Masson's trichrome staining showed that collagen fibers were stained blue, whereas the cell cytoplasm was stained red. Muscle fibers and cell nuclei were stained light pink and dark brown, respectively. The pictures used for the analysis were collected from randomly selected regions.

Western blot analysis. The expression of α-SMA, collagen I, and TGF-β in the HS regions was evaluated using western blot analysis. The HS samples were lysed as previously described (36). The standard bicinchoninic acid method was used to evaluate and prepare the protein samples before immunoblotting. Mouse anti-α-SMA (1:300; cat. no. ab7817; Abcam, Cambridge, UK), anti-GADPH (1:1,000; cat. no. sc32233; Santa Cruz Biotechnology, Dallas, TX, USA), mouse anti-collagen I (1:1,000; cat. no. ab90395; Abcam), and mouse anti-TGF-β 1(1:1,000; cat.

no. ab190503; Abcam) were used as primary antibodies, and goat anti-mouse IgG H&L (1:5,000; cat. no. ab6789; Abcam) was used as secondary antibody. The images were acquired using Amersham Imager 600 (GE Healthcare, Chicago, IL, USA). Densitometric analysis was performed using Image Quant TL software (Cytiva, Marlborough, MA, USA). The expression level of each target protein was determined using ImageJ software (National Institutes of Health, Bethesda, MD, USA) and normalized to the expression of glyceraldehyde 3-phosphate dehydrogenase (GAPDH) protein.

Statistical analysis. The experiments were performed three times and the results are presented as the average mean values and standard deviation (Mean±SD). One-way ANOVA test was used for statistical analysis and $p<0.05$ was considered statistically significant.

Results

Synthesis and characterization of MOF-808 loaded silicone patch. In this study, MOF-808, which were synthesized by hydrothermal reaction, were selected due to their rigidity and stability. Subsequently, a comprehensive examination of MOF-808 was conducted to elucidate its morphology and crystalline characteristics, using SEM and PXRD techniques.
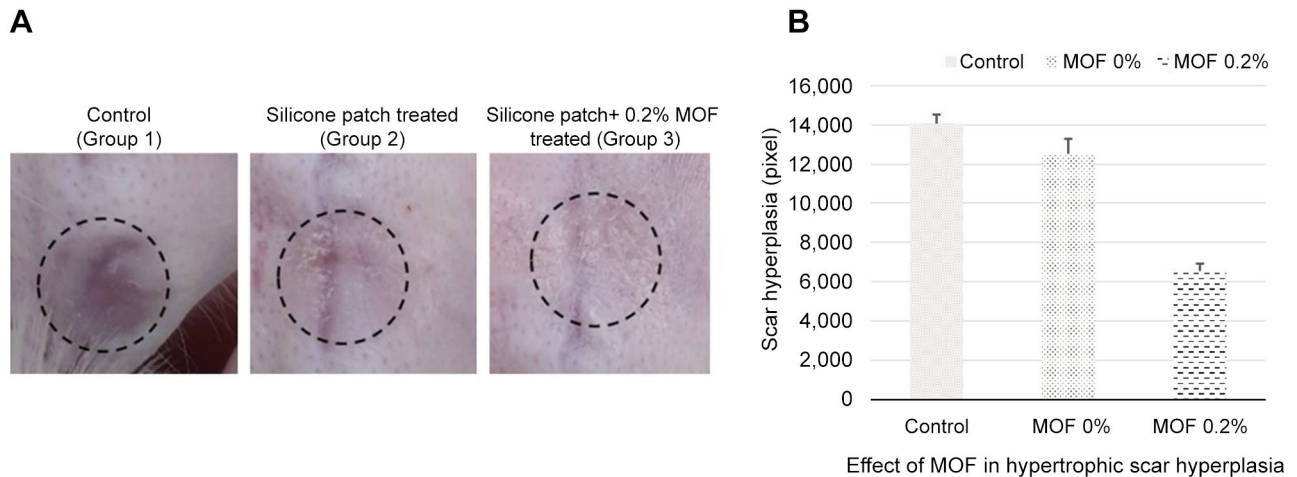
A

B

Effect of MOF in hypertrophic scar hyperplasia

Figure 4. *The examination for the suppression effect of the MOF-808 loaded silicone patch on the hypertrophic scar on day 35 post-generation of the wounds. (A) Observation of the scar texture, visual, and hardness; (B) The rate of scar hyperplasia in control and different MOF-loaded patches groups. The values are presented as the mean±SD (n=3 replicates).*

As shown in Figure 3A, MOF-808, after subjected to a freeze-drying process, had a fine white powder texture and was highly amenable to dispersion within liquid solutions. The MOF-808 has a uniform size of approximately 600 nm and a morphology of octahedral geometry, as shown in Figure 3B. The PXRD images showed sharp peaks of diffraction, demonstrating the high crystalline quality of MOF-808. Also, each diffraction peak correlated with the simulated patterns, indicating that the fabricated product had a structure similar to the predicted one (Figure 3C).

The silicone patch was designed with adhesive properties to enhance its ability to adhere to wounds, thereby extending the contact time and minimizing mobility. To mitigate external influences, half of the adhesive surface was covered with a transparent protective film.

The MOF-808-loaded silicone sheet was fabricated as a film through the uniform blending of polysiloxane, dimethyl silicone oil, silicone resin, a platinum catalyst, and MOF-808. In order to assess the presence and distribution of MOF-808 both on the surface and within the patch, SEM and FIB/SEM analyses were conducted.

As shown in Figure 3D, the MOF-808 loaded silicone sheet exhibits a single-sided adhesive film. Figure 3E and F present SEM images of the 0.2% MOF-loaded silicone patch from both top and side perspectives. SEM analysis revealed that MOF-808 particles were dispersed evenly on the silicone patch, as presented in Figure 3E. Moreover, the uniform distribution of MOF particles was also observed within the silicone layer, situated between the silicone matrix, as shown in Figure 3F. This uniform dispersion both on the surface and within the silicone matrix, contributed to the effective distribution of MOF-808 particles throughout the entire silicone patch.

General features of HS in rabbit models. HS were generated and groped according to different treatments: group 1, the control group without any treatment; group 2, treated with a plain silicone sheet, and group 3, treated with 0.2% MOF-808 loaded silicone sheet. The complete healing duration was set at 2 weeks after the wound generation day. On day 35, the rabbit models were anesthetized, and the macroscopic features of the scar were monitored and photographed in control, silicone patch-treated, and MOF-silicone patch-treated groups. The control group, in which no treatment was administered, showed an apparent red scar with a hard-palpated, thick area at the center. Group 2, the plain silicone patch-treated group, had a lighter color and softer scar, whereas the MOF-silicone patch-applied group showed diminished scar color and resembled normal skin color (Figure 4A). Subsequently, scar hyperplasia was estimated, and a significant reduction in the wound by 11.1 and 53.5% was observed in groups 2 and 3, respectively ($p<0.05$) (Figure 4B).

Histopathological analysis of dermal and epidermal regions of HS. Based on the antifibrotic properties of silicone patches and MOF-loaded silicone patches during HS treatment in rabbit models, we conducted a comprehensive investigation into the alterations and rearrangement of dermal and epidermal thickness.

In the 0.2% MOF-808 loaded sheet treatment group, we observed that the scar was very pale and almost resembled a normal skin, whereas the scar was visible with a hard texture in the untreated control group. On day 35 post-wound generation, the healing process was assessed by measuring the scar widths in all three groups. The results
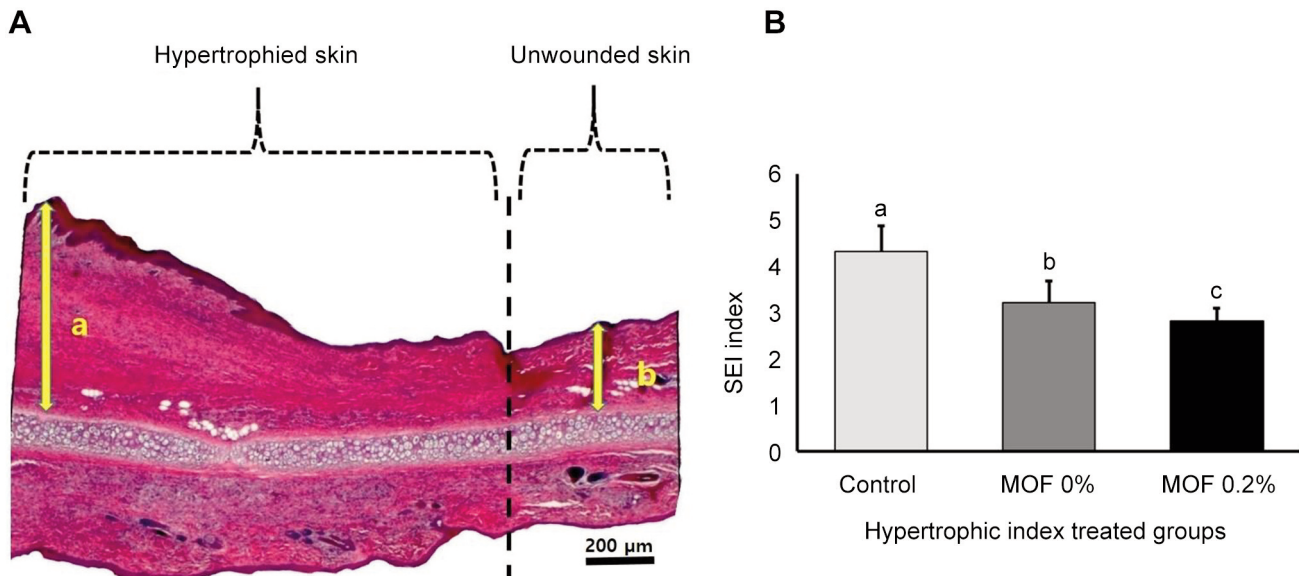
Figure 5. *Histopathological analysis of hypertrophic scar suppression on rabbit ears by 0.2% MOF-loaded silicone patch treatment. (A) Distance between the peak, cartilage area, and normal skin was determined on H&E staining (scale bar is 200 μm); (B) The SEI index was calculated, and a decline of the index values was noticed in the 0.2% MOF-loaded silicone patch group. The statistical significance was set at p<0.05 and the values are presented as the mean±SD (n=3 replicates), and the letters a, b and c indicate statistically significant differences.*

showed significant variation among the three groups. The tissue sections collected on day 35 were analyzed using H&E staining to estimate the SEI ratio (Figure 5A). The calculated SEI value showed that group 3 had a reduced index ratio of 34.6% compared to the control group. A decline in SEI of the silicone patch-treated group 2 was also observed in comparison to group 1, with a decrease by 25.6% (Figure 5B).

Evaluation of epidermal thickness and collagen density. The H&E and Trichrome staining showed that the collagen fibers' density was significantly reduced and fibers were arranged in parallel in 0.2% MOF-loaded silicone patch-treated group. In contrast, the collagen fibers in the control group were dense and disarranged. Figure 6A shows the difference in the epidermis thickness among the three groups. Furthermore, the quantitative analysis results indicated a 49.5% decline in thickness in group 3 compared to group 1 (Figure 6B). Subsequently, Masson's Trichrome staining suggested very dense and disarranged collagen fibers in the control group under the microscope (Figure 6C). Notably, a reduction of 15.7% in collagen density was observed in the MOF-loaded silicone patch-treated group and a 7.5% reduction was noticed in the positive control (plain silicone sheet treatment) group when compared to the control group (Figure 6D). Group 3 exhibited a distinct and notably smoother collagen fiber texture compare to other treatment groups.

Expression of α-SMA, collagen I, and TGF-β in MOF treated Rabbit HS model. To further understand the underlying mechanism responsible for the effects of MOF treatment on scar tissue which suppressed epidermal thickness and collagen density in the rabbit model, we analyzed specific myofibroblast biomarker proteins: α-SMA, collagen I, and TGF-β1, using western blotting. The approximate molecular weight of TGF-β1, col-I, and α-SMA were 25, 35, and 44 kDa, respectively. Western blot analysis was performed for these three proteins and compared to the expression of the GAPDH protein (approximately 36 kDa), which served as the positive control protein across all experimental groups.

Our results showed that the expression levels of α-SMA, collagen I, and TGF-β1 were notably higher in the control group and gradually decreased in both the positive control and MOF-treated groups (Figure 7A).

A significant decrease in the expression of myofibroblast marker proteins was observed in the MOF-loaded silicone patch group, as shown in Figure 7B. To quantify this decline, we calculated the percentage reduction in the expression of α-SMA, collagen I, and TGF-β1 separately in comparison to the control group as outlined in Table I. While there were no statistically significant differences in the expression of collagen I among the control no treatment group, we observed a reduction of 28% and 12.5% in MOF-loaded silicone and plain silicone patch-treated rabbit models, respectively. A significant decline of 40% and 23.4% in α-SMA expression was observed compared to that of the
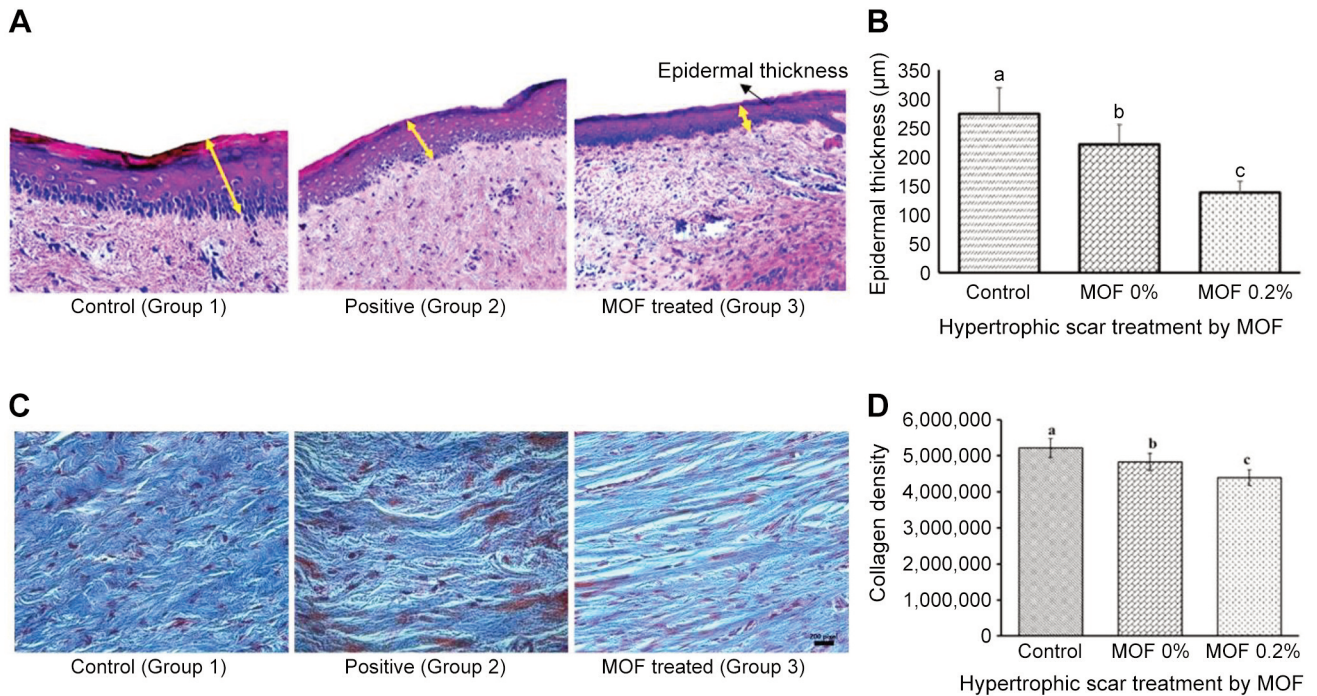
Figure 6. *Reduction of epidermal thickness and collagen fibers after Zr-MOF-808-loaded patches treatment. (A) H&E staining of tissue sections and (B) the graph of the epidermal thickness revealing decreases of the epidermal thickness in positive (0% MOF), and 0.2% MOF -treated groups in comparison with the control (scale bar: 200 μm); (C) Masson Trichrome staining of tissue sections revealed the texture of collagen in each indicated group; (D) A suppression of HS collagen density was observed in the 0.2% MOF treated group. The values are resented as the mean±SD (n=5 replicates), and the alphabet letters (a, b, and c) indicate statistically significant differences p<0.05.*

control group (*p*<0.05). Similarly, a decrease of 20% and 6.7% was observed in the case of TGF- β1 in groups 3 and 2, respectively, compared to group 1. Notably, all scars treated with silicone patches demonstrated a decline in the expression of biomarker proteins as compared to the control group, where no treatment was provided.

Discussion

The hypertrophic scar (HS) is an irregular wound healing process clinically defined by over-production of the collagen and the excess of extracellular matrix (ECM) deposition due to deep dermal injuries (37). Hemostasis, inflammation, proliferation, and tissue remodeling are four stages of wound healing (38). While several therapies for scars have been proposed in the past, only a few of them were followed by further trials with the required control group. In this study, we performed a reproducible study to generate hypertrophic scarring without disrupting the rabbit ear cartilage zone. Furthermore, we investigated the dermal and epidermal thickness, collagen density, SEI ratio, and expression of the marker proteins related to fibrosis.

In recent years, the understanding and advancement of more defined therapeutic options for such lesions have increased in terms of the molecular and biological mechanisms of HS formation (19). A wound with a diameter of 12 mm was found to be the optimal configuration for the generation of HS, which was subsequently utilized for the evaluation of the efficacy of the MOF-silicone patch treatment. A previous study conducted by Kloeters *et al*. (39) in a rabbit ear model suggested that wound with a 7-mm diameter exhibited no observable signs of contraction. Hence, a delay in epithelialization may result in the formation of elevated scars. Furthermore, the documented HS-reducing effects of the MOF-silicone patch on the rabbit ear were replicated in our study with a significant reduction in SEI in the treated wounds. While achieving scarless healing remains the ultimate objective in wound healing, our study acknowledges that the optimal outcome typically involves the formation of a slightly pigmented and flat scar (40). This outcome is associated with a reduction in SEI and epidermal thickness, as well as in the organized alignment of collagen fibers. Thus, our findings support the use of MOF-loaded silicone patches as a promising therapeutic approach for the treatment of HS.

In the context of wound healing, abnormal reactions trigger the proliferation of fibroblasts, resulting in increased collagen synthesis. This process plays a pivotal role in the formation of HS (41). The wound healing process is
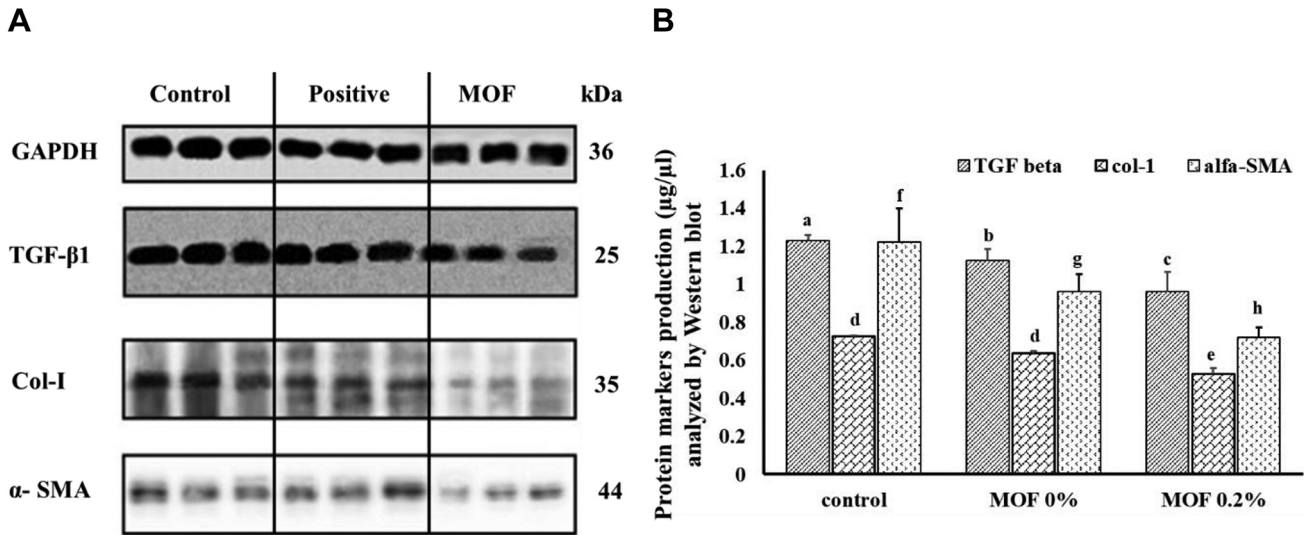
A

B

Figure 7. *Suppression of myofibroblast biomarker proteins in MOF treated HS on rabbit ear. (A) TGF-β1, Collagen-I, and α-SMA protein expression levels were analyzed by western blot using anti-TGF-β1, anti-collagen-1, anti-α-SMA, and anti-GAPDH antibodies, respectively, in all groups. GAPDH: Glyceraldehyde 3-phosphate dehydrogenase; TGF: transforming growth factor; Col: collagen; SMA: smooth muscle actin. (B) The bar graph illustrates the expression levels of each myofibroblasts marker protein. The data are presented as the mean±SD of three replicates, statistical significance was set at p<0.05, and the alphabet letters a-h indicate a statistically significant difference.*

characterized by intricate interactions between profibrotic and antifibrotic molecules, involving a spectrum of mediators, including proteolytic enzymes, growth factors, and extracellular matrix (ECM) constituents (41, 42). Our analytical investigation revealed a direct correlation between enhanced HS treatment and reduced scar hyperplasia, epidermal thickness, collagen density, and the expression of specific marker proteins, ultimately contributing to the restoration of a physiologically regular skin structure.

The HS formation, which is also correlated with increased or prolonged activity of TGF-β1, leads to excessive collagen production and deposition (43), and an increase in expression of α-smooth muscle actin (α-SMA) expression in fibroblasts (44). The skilled phagocytes of apoptotic cells and pieces of matrices are linked to the activation and repression of pro-inflammatory cytokine synthesis by anti-inflammatory mediators (such as TGF-β) (45). Furthermore, TGF-β is released in conjunction with certain matrix proteins, which trigger fibroblasts to become myofibroblasts (46). Although α-SMA expression is a hallmark of mature myofibroblasts, its precise role in wound healing, particularly in the regulation of fibroblast activity, remains incompletely elucidated (47). Here, we have shown conclusive proof of the impact of silicone patches containing MOF-808 on rabbit ear wound healing and HS formation, as well as the interaction of MOF-808 with TGF-1, α-SMA, and collagen I *in vivo*.

Activated myofibroblasts participate in repair by producing significant amounts of ECM proteins, and they may be responsible for the contraction of a healed wound

Table I. *The relative expression level of myofibroblast biomarker protein of each experimental group to the control during HS treatment.*

Marker proteins	Group 2	Group 3
TGF-β1	6.7	20
Col-I	12.5	28
α-SMA	25.4	40

Group 2 is the 0% MOF silicone patch-treated group and Group 3 is the 0.2% MOF-loaded silicone patch-treated group.

(45). The myofibroblasts modulate collagen fibrillogenesis during the remodeling phase and promote collagen breakdown, which reduces myofibroblast adhesion through an apoptotic mechanism (48). Additionally, the HS fibroblasts produce more collagen I, which promotes proliferation (49). In the current study, a decrease in the expression and generation of myofibroblast marker proteins by silicone patches loaded with MOF-808 that were applied to rabbit ears for HS therapy raises the possibility that anti-inflammatory cytokines are involved in controlling and inhibiting scarring. The proteins produced by myofibroblasts play a crucial role in the maintenance of tissue shape and function and are engaged in both intracellular and extracellular processes that result in HS. Although these findings demonstrate the efficiency of MOF in preventing HS, more research is necessary to fully comprehend the MOF mechanism.

Silicone gels have been shown to improve hydration of the stratum corneum and facilitate the regulation of fibroblast proliferation and decreasing collagen synthesis (18). Several studies have demonstrated the role of MOFs in biology and medicine. In drug delivery, MOFs are essential, because they can change functional groups and bio-material pores (50). In addition, MOF products have been successfully used in the adsorption of organic compounds. Therefore, more studies are necessary to assess the efficiency and nano-safety of these material types due to their versatility (51). A study conducted on the nanocarrier system had effectively delivered antitumor and retroviral anti-cancer and AIDS medication by non-toxic, porous iron (III) based MOFs (such as MIL-53, MIL-88, MIL-88Bt, MIL-89, MIL-100, and MIL-101 NH2) (52). Subsequently, Zr-MOF is one of the most promising MOF materials for practical applications due to its rich variety of structures, excellent stability, and intriguing features and functions (53). Incorporating niacin MOFs-encapsulated microcapsules as a therapeutic agent has the potential to significantly enhance the healing of chronic wounds in a model featuring an infected full-thickness skin defect (53). Also, following the rapid and effective endocytosis process, the Zr-MOF remained structurally intact (54). Due to their easy preparation, tunable pores, and the ability to exploit their internal surfaces, MOFs have received considerable attention over the last decade, but prototype frames have exceptional characteristics for use in drug discovery, cancer treatment, gas storage, and many more (55). Hence, in the current study, a silicone and MOF-808 combination was investigated for HS suppression effects in a rabbit ear HS model.

Conclusion

The application of MOFs in practical manufacturing is still challenging because of issues relate to medication quality and metabolism. However, we discovered that our efforts to create a rabbit ear model to suppress the HS production using a silicone patch loaded with MOF-808 were successful. Research on silicone patches containing MOF has revealed anti-HS outcomes by changing the proliferation and remodeling processes involved in wound healing *via* lowering the expression of the epidermal thickness, marker proteins, and SEI, and as well as significant improvement in the organization of collagen. For these reasons, a silicone patch containing MOF-808 can be an effective preventative treatment for HS. Although our findings have a fascinating biological potential, more research is still required.

Conflicts of Interest

The Authors have no conflicts of interest to declare in relation to this study.

Authors' Contributions

Conceptualization: Bakhtiyor Najmiddinov, Xin Rui Zhang, Unjin Ryu: formal analysis, writing, data curation and editing, software, visualization. Kyung Min Choi, Sun-Young Nam, Chan-Yeong Heo: Conceptualization, methodology Supervision, validation, project administration.

Acknowledgements

References

1   Balaraman B, Geddes ER, Friedman PM: Best reconstructive techniques. Dermatol Surg 41(Supplement 10): S265-S275, 2015. DOI: 10.1097/DSS.0000000000000496

2   Martin P, Nunan R: Cellular and molecular mechanisms of repair in acute and chronic wound healing. Br J Dermatol 173(2): 370-378, 2015. DOI: 10.1111/bjd.13954

3   Bloemen MC, van der Veer WM, Ulrich MM, van Zuijlen PP, Niessen FB, Middelkoop E: Prevention and curative management of hypertrophic scar formation. Burns 35(4): 463-475, 2009. DOI: 10.1016/j.burns.2008.07.016

4   Li-Tsang CW, Feng B, Huang L, Liu X, Shu B, Chan YT, Cheung K-K: A histological study on the effect of pressure therapy on the activities of myofibroblasts and keratinocytes in hypertrophic scar tissues after burn. Burns 41(5): 1008-1016, 2015. DOI: 10.1016/j.burns.2014.11.017

5   Yu A, Yick K: Compression and stretch fit garments. In: Engineering of high-performance textiles. Elsevier, pp. 279-303, 2018. DOI: 10.1016/B978-0-08-101273-4.00011-1

6   Dewey WS, Richard RL, Parry IS: Positioning, splinting, and contracture management. Phys Med Rehabil Clin 22(2): 229-247, 2011. DOI: 10.1016/j.pmr.2011.02.001

7   Cho YS, Jeon JH, Hong A, Yang HT, Yim H, Cho YS, Kim D, Hur J, Kim JH, Chun W, Lee BC, Seo CH: The effect of burn rehabilitation massage therapy on hypertrophic scar after burn: A randomized controlled trial. Burns 40(8): 1513-1520, 2014. DOI: 10.1016/j.burns.2014.02.005

8   Nourian Dehkordi A, Mirahmadi Babaheydari F, Chehelgerdi M, Raeisi Dehkordi S: Skin tissue engineering: wound healing based on stem-cell-based therapeutic strategies. Stem Cell Res Ther 10(1): 111, 2019. DOI: 10.1186/s13287-019-1212-2

9   Wynn TA, Ramalingam TR: Mechanisms of fibrosis: therapeutic translation for fibrotic disease. Nat Med 18(7): 1028-1040, 2012. DOI: 10.1038/nm.2807

10 Pohlers D, Brenmoehl J, Löffler I, Müller CK, Leipner C, Schultze-Mosgau S, Stallmach A, Kinne RW, Wolf G: TGF-β and fibrosis in different organs — molecular pathway imprints. Biochim Biophys Acta 1792(8): 746-756, 2009. DOI: 10.1016/j.bbadis.2009.06.004

11 Lichtman MK, Otero-Vinas M, Falanga V: Transforming growth factor beta (TGF-β) isoforms in wound healing and fibrosis. Wound Repair Regen 24(2): 215-222, 2016. DOI: 10.1111/wrr.12398

12 Tang PM, Zhang YY, Mak TS, Tang PC, Huang XR, Lan HY: Transforming growth factor-β signalling in renal fibrosis: from Smads to non-coding RNAs. J Physiol 596(16): 3493-3503, 2018. DOI: 10.1113/JP274492

13 Carthy JM: TGFβ signaling and the control of myofibroblast differentiation: Implications for chronic inflammatory disorders. J Cell Physiol 233(1): 98-106, 2018. DOI: 10.1002/jcp.25879

14 Wei Y, Wang Y, Zhang M, Yan G, Wu S, Liu W, Ji G, Li-Tsang CW: The application of 3D-printed transparent facemask for facial scar management and its biomechanical rationale. Burns 44(2): 453-461, 2018. DOI: 10.1016/j.burns.2017.08.006

15 Ogawa R, Mitsuhashi K, Hyakusoku H, Miyashita T: Postoperative electron-beam irradiation therapy for keloids and hypertrophic scars: Retrospective study of 147 cases followed for more than 18 months. Plast Reconstr Surg 111(2): 547-553, 2003. DOI: 10.1097/01.PRS.0000040466.55214.35

16 Zhang J, Li Y, Bai X, Li Y, Shi J, Hu D: Recent advances in hypertrophic scar. Histol Histopathol 33(1): 27-39, 2018. DOI: 10.14670/HH-11-908

17 Gold MH: Topical silicone gel sheeting in the treatment of hypertrophic scars and keloids. J Dermatol Surg Oncol 19(10): 912-916, 1993. DOI: 10.1111/j.1524-4725.1993.tb00978.x

18 Puri N, Talwar A: The efficacy of silicone gel for the treatment of hypertrophic scars and keloids. J Cutan Aesthet Surg 2(2): 104-106, 2009. DOI: 10.4103/0974-2077.58527

19 Gupta J, Jain V, Jain P: Therapeutic potential of silicone gel sheet treatment and alteration in transforming growth factor beta gene expression in hypertrophic scars. J Med Soc 32(2): 87, 2018.

20 Zhuang JL, Ceglarek D, Pethuraj S, Terfort A: Rapid room-temperature synthesis of metal–organic framework HKUST-1 crystals in bulk and as oriented and patterned thin films. Adv Funct Mater 21(8): 1442-1447, 2011. DOI: 10.1002/adfm.201002529

21 Majano G, Martin O, Hammes M, Smeets S, Baerlocher C, Pérez-Ramírez J: Metal-organic frameworks: Solvent-mediated reconstruction of the metal-organic framework HKUST-1 (Cu$_3$(BTC)$_2$) (Adv. Funct. Mater. 25/2014). Adv Funct Mater 24(25): 3837-3837, 2014. DOI: 10.1002/adfm.201470162

22 Hoskins BF, Robson R: Infinite polymeric frameworks consisting of three dimensionally linked rod-like segments. J Am Chem Soc 111(15): 5962-5964, 1989. DOI: 10.1021/ja00197a079

23 Ōkawa H, Sadakiyo M, Yamada T, Maesato M, Ohba M, Kitagawa H: Proton-conductive magnetic metal-organic frameworks, {NR3(CH2COOH)}[M(a)(II)M(b)(III)(ox)3]: effect of carboxyl residue upon proton conduction. J Am Chem Soc 135(6): 2256-2262, 2013. DOI: 10.1021/ja309968u

24 Zhang W, Lu G, Cui C, Liu Y, Li S, Yan W, Xing C, Chi YR, Yang Y, Huo F: A family of metal-organic frameworks exhibiting size-selective catalysis with encapsulated noble-metal nanoparticles. Adv Mater 26(24): 4056-4060, 2014. DOI: 10.1002/adma.201400620

25 Guo Y, Feng X, Han T, Wang S, Lin Z, Dong Y, Wang B: Tuning the luminescence of metal-organic frameworks for detection of energetic heterocyclic compounds. J Am Chem Soc 136(44): 15485-15488, 2014. DOI: 10.1021/ja508962m

26 Hu Z, Deibert BJ, Li J: Luminescent metal-organic frameworks for chemical sensing and explosive detection. Chem Soc Rev 43(16): 5815-5840, 2014. DOI: 10.1039/C4CS00010B

27 Mason JA, Oktawiec J, Taylor MK, Hudson MR, Rodriguez J, Bachman JE, Gonzalez MI, Cervellino A, Guagliardi A, Brown CM, Llewellyn PL, Masciocchi N, Long JR: Methane storage in flexible metal-organic frameworks with intrinsic thermal management. Nature 527(7578): 357-361, 2015. DOI: 10.1038/nature15732

28 He C, Liu D, Lin W: Nanomedicine applications of hybrid nanomaterials built from metal-ligand coordination bonds: Nanoscale metal-organic frameworks and nanoscale coordination polymers. Chem Rev 115(19): 11079-11108, 2015. DOI: 10.1021/acs.chemrev.5b00125

29 Wu P, Wang J, He C, Zhang X, Wang Y, Liu T, Duan C: Luminescent metal-organic frameworks for selectively sensing nitric oxide in an aqueous solution and in living cells. Adv Funct Mater 22(8): 1698-1703, 2012. DOI: 10.1002/adfm.201102157

30 Horcajada P, Gref R, Baati T, Allan PK, Maurin G, Couvreur P, Férey G, Morris RE, Serre C: Metal-organic frameworks in biomedicine. Chem Rev 112(2): 1232-1268, 2012. DOI: 10.1021/cr200256v

31 Atmaja B, Lui BH, Hu Y, Beck SE, Frank CW, Cochran JR: Targeting of cancer cells using quantum dot-polypeptide hybrid assemblies that function as molecular imaging agents and carrier systems. Adv Funct Mater 20(23): 4091-4097, 2010. DOI: 10.1002/adfm.201000732

32 Horcajada P, Chalati T, Serre C, Gillet B, Sebrie C, Baati T, Eubank JF, Heurtaux D, Clayette P, Kreuz C, Chang J, Hwang YK, Marsaud V, Bories P, Cynober L, Gil S, Férey G, Couvreur P, Gref R: Porous metal-organic-framework nanoscale carriers as a potential platform for drug delivery and imaging. Nature Mater 9(2): 172-178, 2010. DOI: 10.1038/nmat2608

33 Jiang J, Gándara F, Zhang Y-B, Na K, Yaghi OM, Klemperer WG: Superacidity in sulfated metal-organic framework-808. J Am Chem Soc 136(37): 12844-12847, 2014. DOI: 10.1021/ja507119n

34 Harada T, Izaki S, Tsutsumi H, Kobayashi M, Kitamura K: Apoptosis of hair follicle cells in the second-degree burn wound unders hypernatremic conditions. Burns 24(5): 464-469, 1998. DOI: 10.1016/s0305-4179(98)00034-5

35 Guo S, Kang G, Phan DT, Hsu MN, Por YC, Chen CH: Polymerization-induced phase separation formation of structured hydrogel particles *via* microfluidics for scar therapeutics. Sci Rep 8(1): 2245, 2018. DOI: 10.1038/s41598-018-20516-9

36 Mahmood T, Yang PC: Western blot: technique, theory, and trouble shooting. N Am J Med Sci 4(9): 429-434, 2012. DOI: 10.4103/1947-2714.100998

37 Gauglitz GG: Management of keloids and hypertrophic scars: current and emerging options. Clin Cosmet Investig Dermatol 6: 103-114, 2013. DOI: 10.2147/CCID.S35252

38 Reinke J, Sorg H: Wound repair and regeneration. Eur Surg Res 49(1): 35-43, 2012. DOI: 10.1159/000339613

39 Kloeters O, Schierle C, Tandara A, Mustoe TA: The use of a semiocclusive dressing reduces epidermal inflammatory cytokine expression and mitigates dermal proliferation and inflammation in a rat incisional model. Wound Repair Regen 16(4): 568-575, 2008. DOI: 10.1111/j.1524-475X.2008.00404.x

40 Finnerty CC, Jeschke MG, Branski LK, Barret JP, Dziewulski P, Herndon DN: Hypertrophic scarring: the greatest unmet

challenge after burn injury. Lancet 388(10052): 1427-1436, 2016. DOI: 10.1016/S0140-6736(16)31406-4

41 Miller M-C, Nanchahal J: Advances in the modulation of cutaneous wound healing and scarring. BioDrugs 19(6): 363-381, 2005. DOI: 10.2165/00063030-200519060-00004

42 Werner S, Grose R: Regulation of wound healing by growth factors and cytokines. Physiol Rev 83(3): 835-870, 2003. DOI: 10.1152/physrev.2003.83.3.835

43 Shah M, Foreman DM, Ferguson MWJ: Neutralisation of TGF-β1 and TGF-β2 or exogenous addition of TGF-β3 to cutaneous rat wounds reduces scarring. J Cell Sci 108(3): 985-1002, 1995. DOI: 10.1242/jcs.108.3.985

44 Nedelec B, Shankowsky H, Scott PG, Ghahary A, Tredget EE: Myofibroblasts and apoptosis in human hypertrophic scars: The effect of interferon-α2b. Surgery 130(5): 798-808, 2001. DOI: 10.1067/msy.2001.116453

45 Shinde AV, Humeres C, Frangogiannis NG: The role of α-smooth muscle actin in fibroblast-mediated matrix contraction and remodeling. Biochim Biophys Acta Mol Basis Dis 1863(1): 298-309, 2017. DOI: 10.1016/j.bbadis.2016.11.006

46 Leask A: Focal Adhesion Kinase: A key mediator of transforming growth factor beta signaling in fibroblasts. Adv Wound Care (New Rochelle) 2(5): 247-249, 2013. DOI: 10.1089/wound.2012.0363

47 Ibrahim MM, Chen L, Bond JE, Medina MA, Ren L, Kokosis G, Selim AM, Levinson H: Myofibroblasts contribute to but are not necessary for wound contraction. Lab Invest 95(12): 1429-1438, 2015. DOI: 10.1038/labinvest.2015.116

48 Xue M, Jackson CJ: Extracellular matrix reorganization during wound healing and its impact on abnormal scarring. Adv Wound Care (New Rochelle) 4(3): 119-136, 2015. DOI: 10.1089/wound.2013.0485

49 Moulin V, Larochelle S, Langlois C, Thibault I, Lopez-Vallé CA, Roy M: Normal skin wound and hypertrophic scar myofibroblasts have differential responses to apoptotic inductors. J Cell Physiol 198(3): 350-358, 2004. DOI: 10.1002/jcp.10415

50 Keskin S, Kızılel S: Biomedical applications of metal organic frameworks. Ind Eng Chem Res 50(4): 1799-1812, 2011. DOI: 10.1021/ie101312k

51 Ordaz A, Gil E, Hernández-Martínez GR, Thalasso F, Rincón S, Zepeda A: Microrespirometric assessment of the metal-organic framework [Co$_2$(btec)(bipy)(DMF)$_2$]$_n$ ("MOF-Co") to prevent inhibition by arsenic in activated sludge. Env Sc Water Res Technol 6(4): 1153-1162, 2020. DOI: 10.1039/C9EW00967A

52 Horcajada P, Serre C, Maurin G, Ramsahye NA, Balas F, Vallet-Regí M, Sebban M, Taulelle F, Férey G: Flexible porous metal-organic frameworks for a controlled drug delivery. J Am Chem Soc 130(21): 6774-6780, 2008. DOI: 10.1021/ja710973k

53 Chen G, Yu Y, Wu X, Wang G, Gu G, Wang F, Ren J, Zhang H, Zhao Y: Microfluidic electrospray niacin metal-organic frameworks encapsulated microcapsules for wound healing. Research (Wash D C) 2019: 6175398, 2019. DOI: 10.34133/2019/6175398

54 Bai Y, Dou Y, Xie L-H, Rutledge W, Li J-R, Zhou H-C: Zr-based metal-organic frameworks: design, synthesis, structure, and applications. Chem Soc Rev 45(8): 2327-2367, 2016. DOI: 10.1039/C5CS00837A

55 Bradshaw D, Garai A, Huo J: Metal-organic framework growth at functional interfaces: thin films and composites for diverse applications. Chem Soc Rev 41(6): 2344-2381, 2012. DOI: 10.1039/C1CS15276A

56 Granadeiro CM, Ribeiro SO, Karmaoui M, Valença R, Ribeiro JC, de Castro B, Cunha-Silva L, Balula SS: Production of ultra-deep sulfur-free diesels using a sustainable catalytic system based on UiO-66(Zr). Chem Commun 51(72): 13818-13821, 2015. DOI: 10.1039/C5CC03958D